Analytical Biochemistry 423 (2012) 277–285

Contents lists available at SciVerse ScienceDirect

Analytical Biochemistry

journal homepage: www.elsevier.com/locate/yabio

An impedimetric vascular endothelial growth factor biosensor-based PAMAM/cysteamine-modified gold electrode for monitoring of tumor growth

Mustafa Kemal Sezgintürk [a,*], Zihni Onur Uygun [b]

[a] Namık Kemal University, Faculty of Science, Chemistry Department, Biochemistry Division, Tekirdağ, Turkey
[b] Çanakkale Onsekiz Mart University, Faculty of Science, Chemistry Department, Çanakkale, Turkey

ARTICLE INFO

Article history:
Received 15 September 2011
Received in revised form 5 December 2011
Accepted 29 December 2011
Available online 8 January 2012

Keywords:
VEGF
Tumor growth
VEGF-R1
PAMAM
Electrochemical impedance spectroscopy
Biosensor

ABSTRACT

In the present work, we have developed a new biosensor based on fourth-generation (G4) PAMAM dendrimers for the analysis of vascular endothelial growth factor (VEGF). First, the PAMAM dendrimers were covalently attached to a cysteamine-modified Au electrode by glutaraldehyde. With the help of the amino groups located on its surface, vascular endothelial growth factor receptor-1 (VEGF-R1) was immobilized via glutaraldehyde cross-linking. VEGF-R1 loading was investigated to identify the optimal VEGF-R1 immobilization conditions for the best sensitivity of the new biosensor. In addition, Kramers–Kronig transforms were also analyzed for immobilization and measurement processes. The biosensor had a linear range of 5 to 125 pg/mL VEGF. The fabricated biosensor had good repeatability and reproducibility. Finally, the results for artificial serum samples measured by the present biosensor showed a good recovery for VEGF detection.

Vascular endothelial growth factor (VEGF)[1] is an angiogenic growth factor. VEGF is also known as vasculotropin, and stimulates endothelial cell growth, angiogenesis, and capillary permeability. Angiogenesis is the key process in tumor growth, progression, and metastasis. VEGF regulates angiogenesis physiologically and pathophysiologically [1–6]. Moreover, the growth of structurally chaotic and functional anomalous vessels into a tumor burden is promoted by VEGF [7–9]. Preclinical and clinical settings first verified the importance of VEGF in breast cancer [10–13]. In the preclinical studies it was demonstrated that breast cancer cells expressing VEGF enhanced the growth and metastatic potential of human tumors. In the clinical setting the results were more disastrous: VEGF overexpression in the early stage revealed a significant metastasis [14–17]. The statistical throughputs revealed that, in women, breast cancer is the second most common cancer type to be faced. According to the reports of the American Cancer Society, about 1.3 million women will be diagnosed with breast cancer annually worldwide, and about 465,000 will die from the disease [18,19].

The subject of the study is to develop an electrochemical biosensor system based on electrochemical impedance spectroscopy. This will enable fast, sensitive, and practical determination of the breast cancer biomarker, VEGF, which is often encountered in the clinical field and poses a threat to many people, especially women. Previously, a number of determination systems for VEGF have been reported. For example, the technology of semiconductor nanowire-based sensor systems has been developed for detection of VEGF [20–26]. Lee and co-workers reported label-free and electrical detection of VEGF using anti-VEGF aptamer-modified Si nanowire field-effect transistors [27]. Prabhulkar and co-workers also reported a biosensor based on ferrocene monocarboxylic acid-labeled anti-VEGF, which was covalently immobilized on a microelectrode surface [28]. The biosensor allowed VEGF analysis with a detection limit of about 38 pg/mL.

Recently, EIS has become an efficient method used for many chemical and physical processes. EIS presents analytic solutions for many processes. Besides these, identification of membranes, biosensor characterization, and fabrication can also be effectively monitored by EIS. In addition, enzyme–substrate interactions after antigen–antibody, receptor–ligand, or DNA–DNA interactions, which have no catalytic reaction, could be successively monitored by EIS [29–31]. In the current study, human vascular endothelial growth factor receptor 1 (VEGFR1, Flt-1) was used as a bio-recognition element for the first time. Recombinant human VEGF-R1 is a disulfide-linked dimeric protein with two 905 amino acid residue polypeptides, and has a predicted monomeric molecular mass of 100 kDa [32–34]. The recombinant soluble VEGF-R1 binds VEGF with high affinity [35–37].

Cysteamine self-assembled monolayers (SAM) were self-assembled on the gold electrodes. Following that, PAMAM dendrimer

* Corresponding author. Fax: +90 282 293 41 49.
E-mail addresses: msezginturk@hotmail.com, msezginturk@nku.edu.tr (M.K. Sezgintürk).

[1] *Abbreviations used:* BSA, bovine serum albumin; SAM, self-assembled monolayers, VEGF, vascular endothelial growth factor; VEGF-R1, Flt-1, human vascular endothelial growth factor receptor-1.

0003-2697/$ - see front matter © 2012 Elsevier Inc. All rights reserved.
doi:10.1016/j.ab.2011.12.049

was covalently attached to the amino end of the cysteamine with the help of glutaraldehyde. Next, VEGF-R1 was immobilized on PAMAM dendrimers via glutaraldehyde. Using cyclic voltammetry and electrochemical impedance investigations, we demonstrated that the immobilization steps had been achieved. For analyzing EIS data it is fitted to the equivalent circuit model. Certain important parameters were optimized to obtain the best results. Finally, the artificial serum samples spiked with VEGF were analyzed by the biosensor.

Materials and methods

Materials

All reagents were obtained from Sigma–Aldrich (St. Louis, MO, USA). VEGF receptor-1 (Flt-1)/Fc chimera (human) and vascular endothelial growth factor (human) were also obtained from Sigma–Aldrich. VEGF, VEGFR, 0.1% BSA (bovine serum albumin) were prepared in 50 mM, pH 7, phosphate buffer, according to the literature [Jonathan and Daniels, 2007]. PAMAM-25% (G2, C_{12} dendrimer) and 5% glutaraldehyde solutions were prepared in 50 mM, pH 6.8, phosphate buffer. VEGF-R1 and VEGF solutions were stored at −20 °C until use. Synthetic serum solution was prepared by using 4.5 mM KCl, 5 mM $CaCl_2$, 1.6 mM $MgCl_2$, 4.7 mM D(+)-glucose, 2.5 mM urea, 0.1% human serum albumin, and 145 mM NaCl. A redox probe solution was prepared in 50 mM, pH 7, phosphate buffer which contained 0.1 M KCl, 5 mM $Fe(CN)_6^{4-}$, and 5 mM $Fe(CN)_6^{3-}$. Gold working electrodes (1.6 mm^2 surface area), Ag/AgCl reference electrode, and Pt counter electrode were obtained from BASi (Warwickshire, UK). Electrochemical experiments were carried out by using a Compactstat with integrated impedance analyzer (Ivium Technologies, Eindhoven, The Netherlands) interfaced with a PC. All electrochemical experiments were carried out in a Faraday cage (from iBAS, Warwickshire, UK) to block out external static electric fields.

Methods

VEGF-R1 immobilization procedure

Before the VEGF-R1 immobilization, the gold electrodes were first polished with 0.05 μm alumina powder and then washed with ultrapure water. Following that, the electrodes were ultrasonically washed in absolute ethanol for 2 min to remove alumina residues. Then the electrodes were immediately dried with an argon stream for further modifications. In the next step, the electrode was immediately immersed in a cysteamine solution (0.1 M, in pure ethanol) for an hour. After this period, it was rinsed with ethanol and gently dried with an argon stream. The electrodes modified with cysteamine (Au/Cys) were immersed into 5% glutaraldehyde solution for 5 min to activate the amino ends of the cysteamine. At the end of this period the electrode was washed with pH 6.8 phosphate buffer, dried in an argon stream, and immediately immersed into

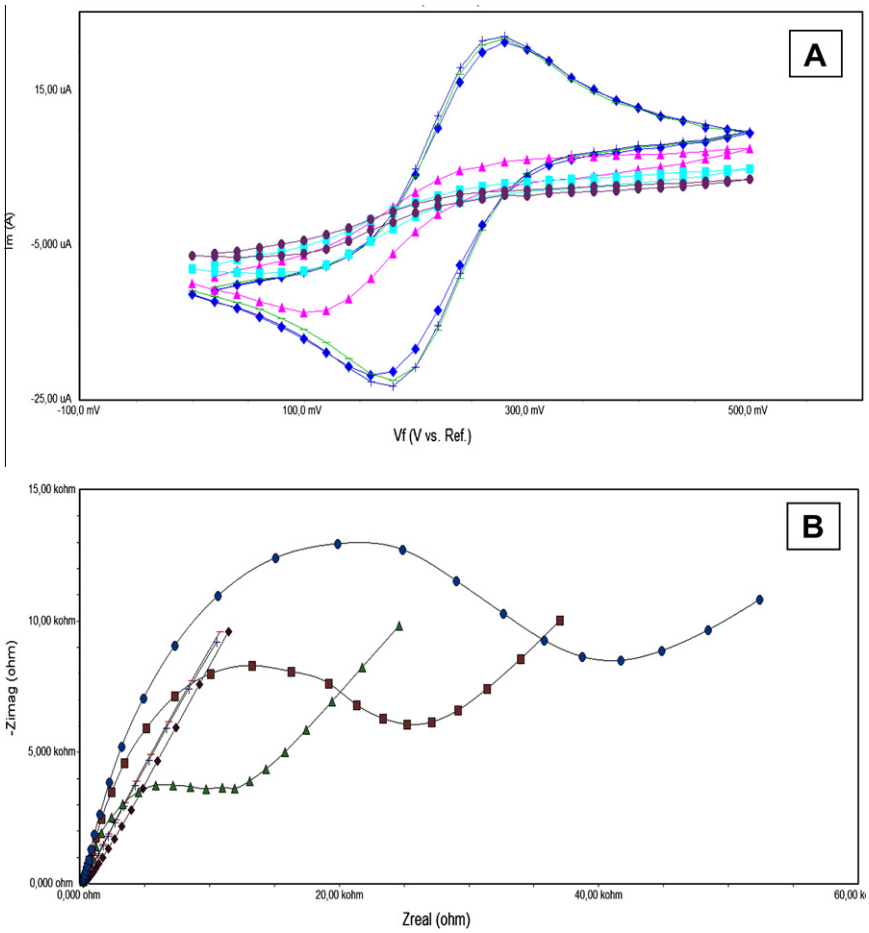

Fig.1. Electrochemical characterization of the biosensor. [(A) Cyclic voltammograms of VEGF-R1 immobilization by PAMAM dendrimers and cysteamine SAMs: -◆-◆-:, bare gold electrode; -_-_-:, Au/Cys; -+-+-:, Au/Cys/PAMAM; -▲-▲-:, Au/Cys/PAMAM/VEGF-R1; -■-■-:, Au/Cys/PAMAM/VEGF-R1/BSA; -●-●-:, Au/Cys/PAMAM/VEGF-R1/BSA/VEGF. (B) Electrochemical impedance spectra of VEGF-R1 immobilization steps: -◆-◆-:, bare gold electrode; -_-_-:, Au/Cys; -+-+-:, Au/Cys/PAMAM; -▲-▲-:, Au/Cys/PAMAM/VEGF-R1; -■-■-:, Au/Cys/PAMAM/VEGF-R1/BSA; -●-●-:, Au/Cys/PAMAM/VEGF-R1/BSA/VEGF.]

PAMAM solution for 30 min. Following that, the PAMAM-modified electrode (Au/Cys/PAMAM) was washed with phosphate buffer (pH 6.8) and dried gently. In order to covalently attach VEGF-R1 to PAMAM the electrodes (Au/Cys/PAMAM) were immersed into glutaraldehyde solution (5%) for 5 min. Then they were washed and dried as noted above. Finally 10 μL of VEGFR-1 solution was dropped onto the activated electrode surface and incubated for 2 h in a humid environment. After washing the surface of the electrode, 10 μL BSA solution (0.1%) was dropped onto the electrode to block the active ends on the surface.

Measurement procedure

Cyclic voltammetry was used to characterize the layer-by-layer formation of the biosensors. The potential was varied between 0 and 500 mV (step size, 20 mV; scan rate, 50 mV/s) in the presence of 5 mM $K_3[Fe(CN)_6]/K_4[Fe(CN)_6]$ (1/1) solution, which served as a redox probe containing 0.1 M KCl. For electrochemical impedance studies, an alternating wave with 10 mV of amplitude was applied to the electrode over the formal potential of the redox couple (0.18 V). The redox couple used for impedance studies was the same as that used in cyclic voltammetry. Impedance spectra were collected in the frequency range between 10,000 and 0.05 Hz.

After each of the VEGF-R1 biosensors was assembled, the biosensor surface was used to interact with the VEGF solution. The standard solution of VEGF was injected over the biosensor surface by a micropipette. For each time measurement, the injection volume was 5 μL. The response value was read after a 1-h incubation in a moisture medium. After this incubation period, the biosensor was gently immersed into the ultrapure water 10 times to remove physically adsorbed VEGF molecules. Finally, the biosensor was again put into the cell containing the $Fe(CN)_6^{4-/3-}$ redox probe solution and the electrochemical measurements were made as described previously. The difference in charge transfer resistance between the biosensor's unbounded and bounded VEGF was used to prepare VEGF calibration curves.

Results and discussion

VEGF-R1 immobilization by cysteamine and PAMAM dendrimers

A well-defined characteristic voltammogram of the redox couple could be observed on the bare gold electrode (Fig. 1A). It was expected that after cysteamine and PAMAM modifications the cyclic voltammograms would remain almost the same as the bare gold

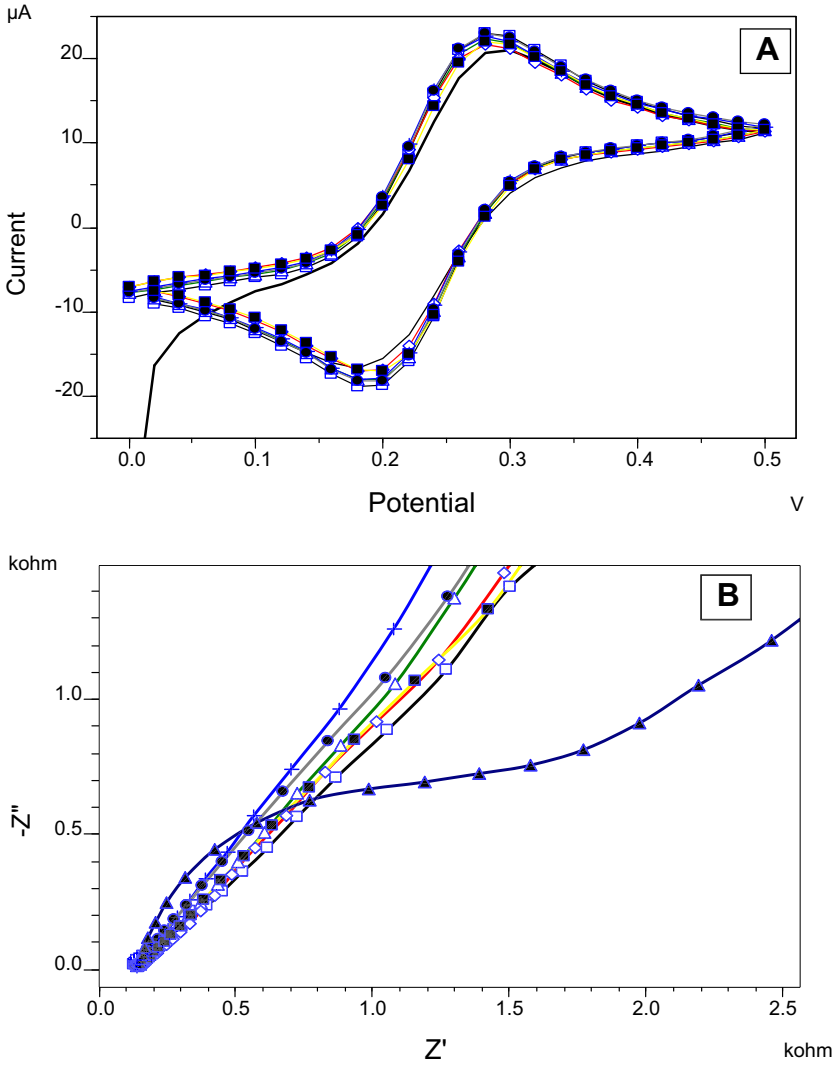

Fig.2. The effect of cysteamine incubation period for SAM formation on gold electrodes. [(A) Cyclic voltammograms related different incubation periods: straight line, bare gold electrode; -■-■-;, 1 h; -●-●-;, 2 h; -+-+-;, 3 h; -◊-◊-;, 4 h; -Δ-Δ- ;, 5 h; -□-□-;, 6 h. (B) Electrochemical impedance spectra obtained for different cysteamine incubation periods: -▲-▲-;, bare gold electrode; -■-■-;, 1 h; -●-●-;, 2 h; -+-+-;, 3 h; -◊-◊-;, 4 h; -Δ-Δ- ;, 5 h; -□-□-;, 6 h.]

electrode. There were no significant changes in the anodic and cathodic currents related to the electrode surfaces. However, after VEGF-R1 modification the cathodic and anodic currents were considerably decreased by the blocking effect of VEGF-R1. Moreover, bovine serum albumin, which was used to block active PAMAM ends, also decreased the peak currents through the same effect of VEGF-R1. These decreases in peak currents were attributed to the fact that VEGF-R1 and BSA insulated the surface and effectively hindered the transfer of electrons toward the electrode surface.

The impedance changes of the modified gold electrode accompanying the stepwise modification process are shown in Fig. 1B. The complex impedance is displayed as the sum of the real and imaginary components (Z_{re} and Z_{im}). The monolayer was treated as a resistor (R_{ct}) and capacitor in parallel, the solution resistance was represented by a resistor, and the Warburg impedance was noticeable at low frequencies. As can be seen from Fig. 1B, after the cysteamine monolayer was self-assembled on the electrode, the interfacial electron transfer resistance R_{ct} was almost the same as that of the bare gold electrode. When the cysteamine-modified electrode was further modified with the PAMAM dendrimer layer, due to the protonated amino ends of PAMAM dendrimer at pH 7, the R_{ct} was almost the same as that of the bare gold electrode and cysteamine-modified electrode. After VEGF-R1 molecules were attached to the PAMAM-modified electrode, the charge transfer resistance was significantly increased in comparison with the previous modified electrode surfaces. This increase indicated the successful immobilization of VEGF-R1 on the gold electrode modified with cysteamine and PAMAM dendrimers. In the last step of VEGF-R1 immobilization, the electrode surface was fabricated with the bovine serum albumin to block active PAMAM ends. As expected, this caused a further increase in R_{ct}.

Optimization parameters for the biosensor

The fabrication steps of the VEGF-R1-based biosensor were examined in terms of incubation periods for cysteamine SAM formation, PAMAM modification, and VEGF-R1 and VEGF bindings. Details are given in the sections below.

The incubation period for cysteamine SAM formation did not significantly affect the response. In order to assess the effect of

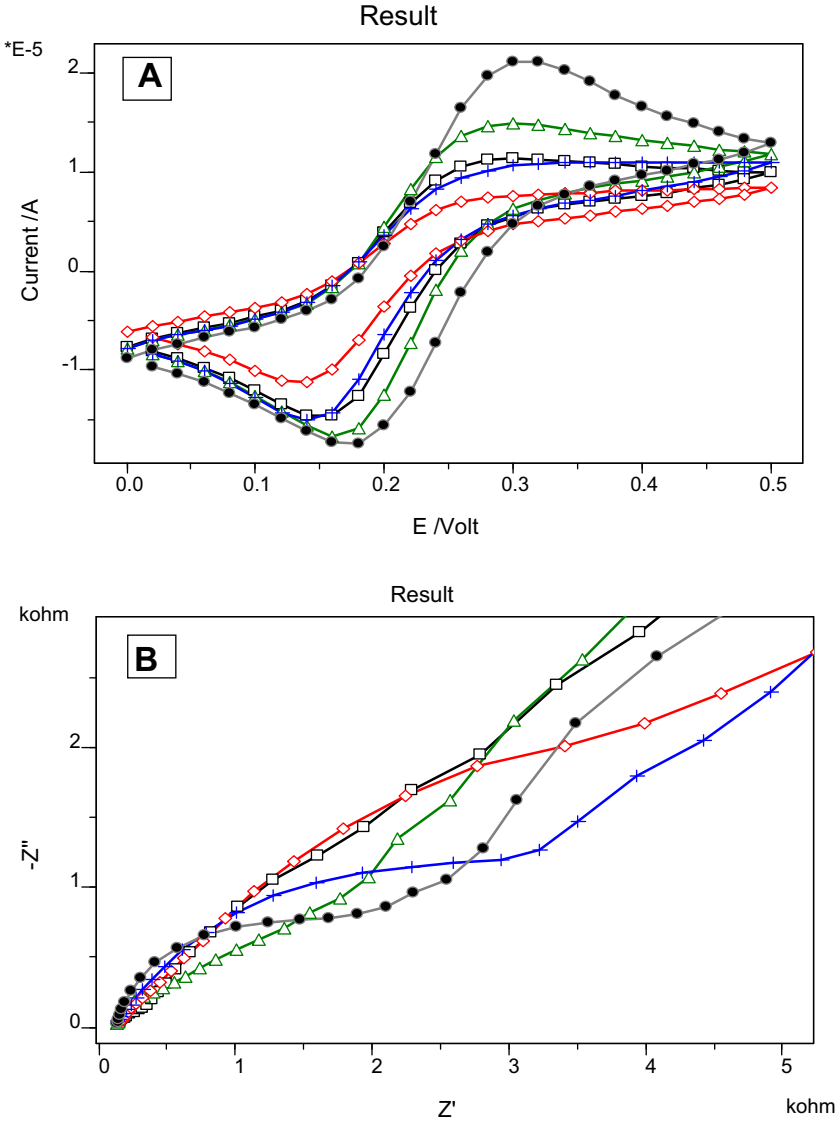

Fig.3. Optimization of PAMAM incubation time for PAMAM modification of gold electrodes self-assembled monolayered by cysteamine. [(A) cyclic voltammograms related different incubation periods: -●-●-:, bare gold electrode; -Δ-Δ- :, 30 min; -□-□-:, 60 min; -+-+-:, 90 min; -◊-◊-:, 120 min. (B) Electrochemical impedance spectra obtained for different cysteamine incubation periods: -Δ-Δ- :, bare gold electrode; -●-●-:, 30 min; -+-+-:, 60 min; -◊-◊-:, 90 min; -□-□-:, 120 min.]

the period for the SAM the biosensors were constructed using different incubation periods: 1, 2, 3, 4, 5, and 6 h (Fig. 2A and B).

The results showed that the increase in the incubation period did not change the CVs and impedance spectra. Moreover, charge transfer resistances belonging to the different incubation periods also did not change by increasing the time. Consequently, to decrease the total immobilization duration, 1 h was chosen, since this was the optimum period for the formation of cysteamine SAM.

The behavior of the biosensor was studied against different PAMAM incubation periods after glutaraldehyde activation of cysteamine amino terminals. Thus, sets of biosensors were prepared for comparison in different incubation periods for PAMAM binding. The obtained cyclic voltammograms and impedance spectra are shown in Fig. 3A and B.

An increase in the PAMAM incubation period resulted in a decrease in peak currents, which could be seen in cyclic voltammograms. Moreover, increasing the incubation period increased the charge transfer resistances. This increase in R_{ct} was associated with the blocking behavior of the PAMAM layer on the electrode surface for the $Fe(CN)_6^{3-/4-}$ redox probe. This effect also contributed to an increase of the semicircle diameter, as can be seen from Fig. 3B. However, according to the results there was no significant difference between the periods of 30 and 60 min. Moreover, in order to decrease the time for total VEGF-R1 immobilization a period of 30 min was chosen, since this was the optimum period of PAMAM incubation.

The next step in the optimization studies was the investigation to establish the VEGF-R1 incubation time needed for effectively binding of VEGF-R1 to PAMAM by glutaraldehyde. For this purpose, four different periods were used to bind VEGF-R1 to PAMAM dendrimer. As can be seen from the cyclic voltammograms, an increase in the incubation period decreased the peak currents.

From Fig. 4B, it can be seen that increasing the incubation period increased the interfacial electron transfer resistance compared with the lower incubation periods. This was because of the more effective blocking behavior of VEGF-R1 toward electron transfer.

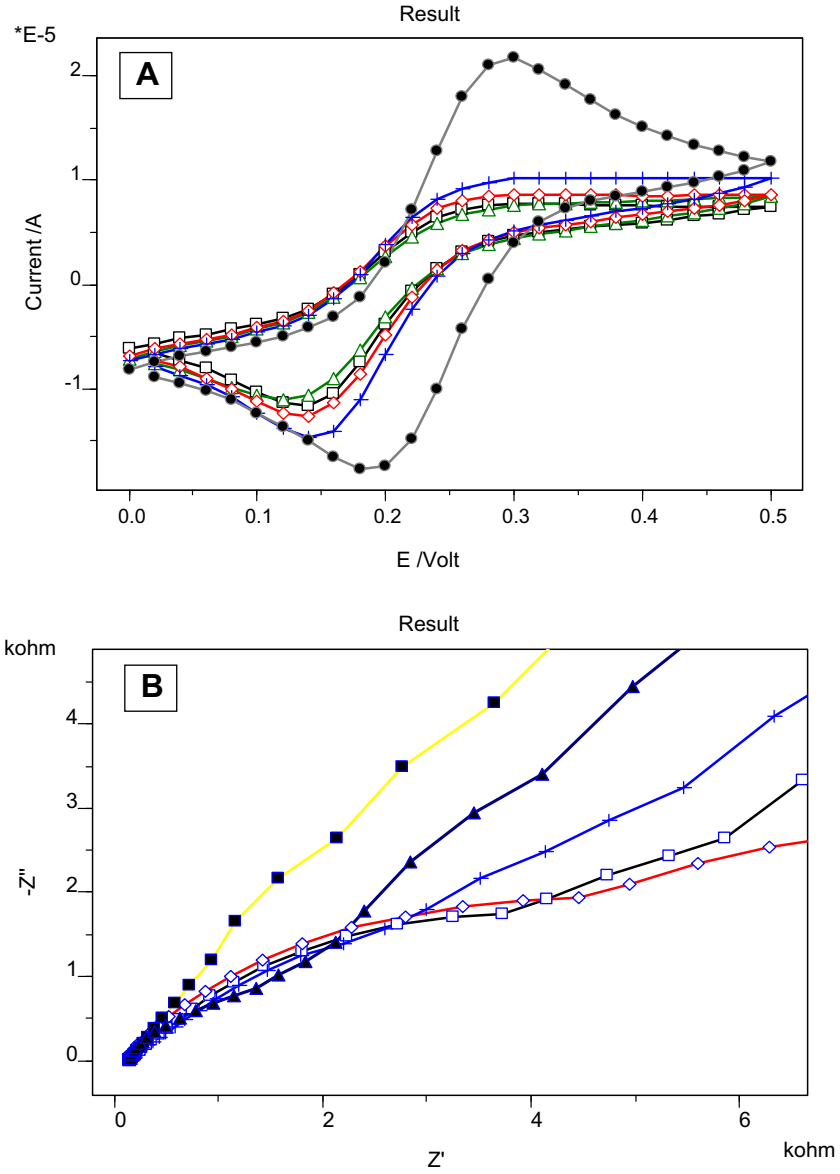

Fig.4. Evaluation of the effect of VEGF-R1 incubation period on the biosensor response. [(A) cyclic voltammograms related different incubation periods: -●-●-; bare gold electrode; -+-+-; 1 h; -◊-◊-; 2 h; -□-□-; 3 h; -Δ-Δ- ; 4 h. (B) Electrochemical impedance spectra obtained for different VEGF-R1 incubation periods: -■-■-; bare gold electrode; -◊-◊-; 4 h; -□-□-; 3 h; -+-+-; 2 h; -▲-▲-; 1 h.]

Moreover, the charge transfer resistances obtained for 2, 3, and 4 h were very close to each other. As a result, in further biosensors an incubation period of 2 h was used for VEGF-R1 binding.

At the end of the optimization studies, the incubation period for binding between VEGF-R1 and VEGF was optimized. For this purpose VEGF-R1/VEGF interaction was realized by using different incubation periods such as 1, 2, 3, and 4 h. The cyclic voltammograms and the impedance spectra are given in Fig. 5A and B. The binding ratio of VEGF to VEGF-R1 was decreased with an increase in the incubation period. The cyclic voltammograms showed that peak currents were considerably reduced by a decrease in the incubation period. However, the charge transfer resistances, R_{ct}, decreased considerably with the increase in incubation time.

From the above, it was demonstrated that an increase in incubation time resulted in ineffective binding of VEGF to VEGF-R1. At the end of the fourth hour of the incubation period, VEGF solution on the electrode surface had completely evaporated spontaneously, although the electrode was incubated in a moisture medium. A similar result was also obtained for the 3-h incubation. It is probable that the binding performance of VEGF to VEGF-R1 was negatively affected due to the long incubation time. However, it seemed that incubation periods shorter than 2 h caused the VEGF solution to evaporate partially. The highest R_{ct} value was obtained after an hour of incubation. Finally, according to the results obtained, it was found most efficient to incubate VEGF for an hour. Finally, because of that the most effective period for VEGF incubation was an hour long. If VEGF-R1 and VEGF incubation periods are evaluated in terms of total measurement duration, short periods for both incubation processes should be favorable.

Analytical characterization of the biosensor

In this study, electrochemical impedance spectroscopy was used to determine the amount of redox probe associated with changes in the electron transfer resistance at the VEGF-R1 biosensor. The charge transfer resistances related with the VEGF concentrations were calculated by the potentiostate system software. However, the equation:

$$R_{ct} = RT \times (n^2F^2AK_{ct}[S])^{-1}$$

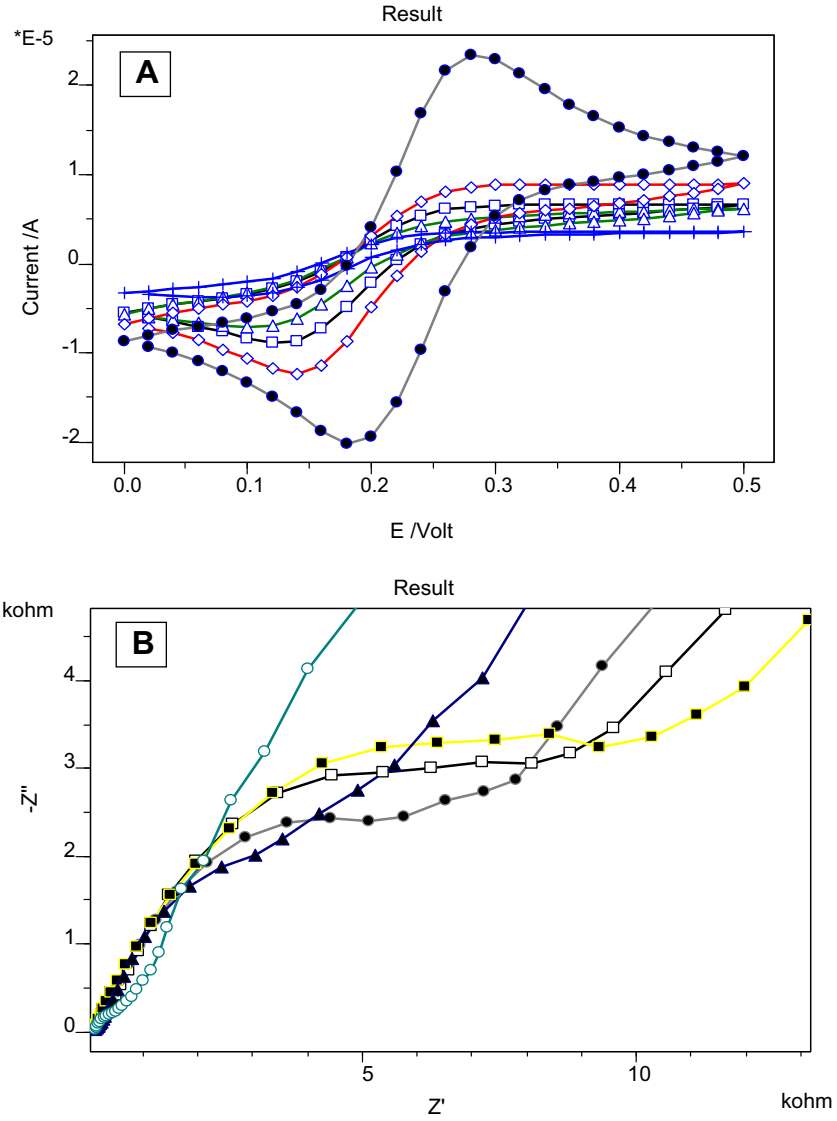

Fig.5. The effect of VEGF incubation period on the biosensor performance. [(A) cyclic voltammograms obtained for different incubation periods: -●-●-; bare gold electrode; -◊-◊-; 4 h; -□-□-; 3 h; -Δ-Δ- ; 2 h; -+-+-; 1 h. (B) Electrochemical impedance spectra obtained for different VEGF incubation periods: -●-●-; bare gold electrode; -■-■-; 1 h; -□-□-; 2 h; -●-●-; 3 h; -▲-▲-; 4 h.]

may be used to explain the charge transfer resistance [30,38,39], where R is the ideal gas constant, T is the absolute temperature, n is the number of transferred electrons per molecule of the redox probe, F is the faraday constant, A is the geometric surface area of the electrode (cm^2), k_{ct} is the potential-dependent charge transfer rate constant, and [S] corresponds to the concentration of the redox probe (mol/cm^3). To obtain a calibration curve of the biosensor we used the variation of the absolute impedance that was calculated by the equation:

$$\Delta R_{ct} = R_{ct}(\mathrm{VEGF-R1/VEGF}) - R_{ct}(\mathrm{VEGF-R1}),$$

where $R_{ct(VEGF-R1/VEGF)}$ is the value of the charge transfer resistance after VEGF-R1 is coupled to VEGF, while $R_{ct(VEGF-R1)}$ is the value of the charge transfer resistance when VEGF-R1 is immobilized on the electrode. As can be seen from Fig. 6A, peak currents decreased with an increase in the concentrations of VEGF standard solutions.

Fig. 6B shows the Nyquist plots evaluation of the biosensor for different VEGF concentrations. It was observed that the semicircle diameter in the Nyquist plots increased with increasing VEGF concentration. Moreover, the low frequencies could be used for concentration-dependent measurements. The impedance spectra should be fitted with an equivalent circuit model as shown in Fig. 7 where the capacitance C_{dl} is the double-layer capacitance, R_{ct} is the charge transfer resistance in low frequency, Z_w is the Warburg element, and R_s is the resistance of the electrolyte and all the connections.

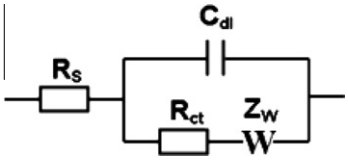

Fig. 7. Equivalent circuit model applied to fit the impedance measurements. [R_s, the ohmic resistance of the electrolyte solution; C_{dl}, associated with the double-layer capacitance; R_{ct}, the electron transfer resistance, and Z_w, the Warburg impedance.]

The increment of VEGF concentration increased the charge transfer resistance, R_{ct}, achieving a linear range between 5 and 125 pg/mL. A calibration graph for VEGF was prepared with the help of the differences in charge transfer resistances after VEGF binding. The calibration curve is given in Fig. 8.

In this work, the new biosensor based on the PAMAM dendrimers system was also analyzed by Kramers–Kronig transforms. The Kramers–Kronig relations are integral equations that constrain the real and imaginary components of complex quantities for systems that satisfy conditions of linearity, causality, and stability [40–42]. In principle, the Kramers–Kronig relations can be used to determine whether the impedance spectrum of a given system has been influenced by bias errors caused, for example, by instrumental artifacts or time-dependent phenomena [42]. The

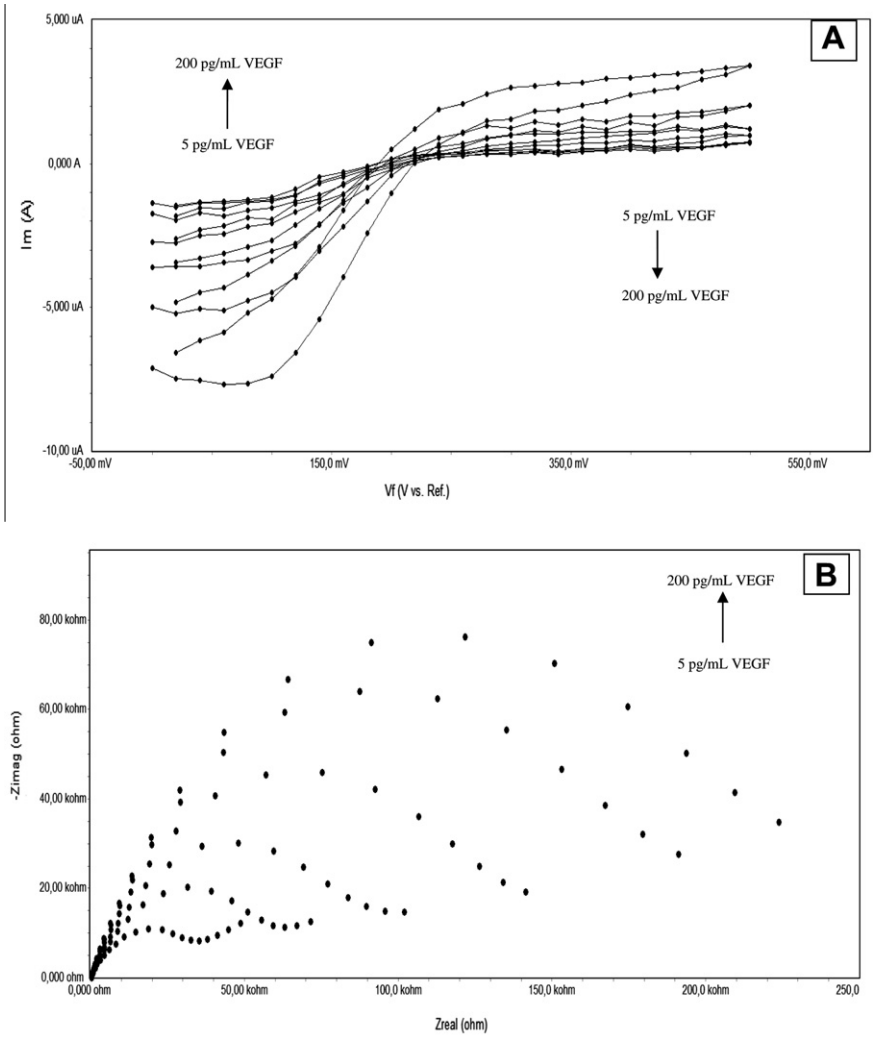

Fig.6. Biosensor responses obtained for different concentrations of vascular endothelial growth factor [cyclic voltammograms (A) and impedance spectra (B)].

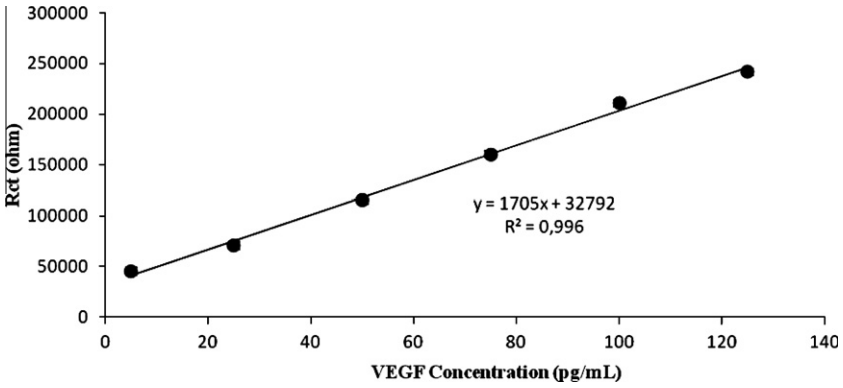

Fig. 8. VEGF calibration curve obtained by the biosensor-based VEGF-R1 immobilized by PAMAM dendrimers and cysteamine SAMs.

Table 1
The analysis of Kramers-Kronig Transforms, Reproducibility, and the sample analysis of the biosensor.

Kramers–Kronig transforms for different layers of the biosensor			
Biosensor surfaces		Goodness of fit values	
Bare Au		1.25	
Au/cysteamine		2.87	
Au/cysteamine/PAMAM		8.45	
Au/cysteamine/PAMAM/VEGF-R1		4.94	
Au/cysteamine/PAMAM/VEGF-R1/VEGF		1.11	
Reproducibility of the biosensor-based PAMAM dendrimers			
Biosensor numbers	R^2	*y*	Linear ranges (pg/mL)
1	0.9978	1662*x* + 12,151	5–125
2	0.9983	1944.6*x* + 37,341	5–125
3	0.9974	1615.2*x* + 35,982	5–125
4	0.9968	1855.4*x* + 42,743	5–125
5	0.9994	1661.1*x* + 45,219	5–125
6	0.986	1560.7*x* + 33,716	5–125
7	0.9995	1362.7*x* + 7328	5–125
8	0.9984	1062.5*x* + 41,744	5–125
9	0.9996	1437.8*x* + 54,479	5–125
10	0.9991	1137.4*x* + 52,707	5–125
11	0.999	1035.9*x* + 56,087	5–125
12	0.9995	1454.5*x* + 57,734	5–125
VEGF detection in artificial serum samples			
VEGF (pg/mL)			
Added	Found by the biosensor*	% Recovery	% Relative difference
20	20.18	100.9	0.9
40	40.31	100.8	0.8
60	60.1	100.2	0.2

* Average values obtained by duplicate measurements.

Kramers–Kronig relations have been applied to electrochemical systems by direct integration of the equations, by experimental observation of stability and linearity, by regression of specific electrical circuit models, and by regression of generalized measurement models [43,44]. Direct integration of the Kramers–Kronig relations involves calculating one component of the impedance from the other, e.g., the real component of impedance from the measured imaginary component. The result is compared to the experimental values obtained [42]. Calculations were carried out following the method of Boukamp [45].

According to these calculations, a value named "goodness of fit" was obtained. In addition, a plot of the relative errors ($\Delta Z/Z$) for the real and imaginary parts of the experimental data was also drawn. For the present new biosensor, for all steps including preparation of the biosensor and measurement, Kramers–Kronig transforms were performed. The goodness of fit values of different biosensor surfaces are also given in Table 1.

The Kramers–Kronig transforms performed on the electrochemical impedance spectra related to the biosensor proved that the experimental data agreed with the data obtained by the transforms (the spectra related were not shown). Moreover, as can be seen from Table 1, goodness of fit values demonstrated that the impedance spectra were linear, stable, and formed a causal circuit. Finally, these data also showed that the system was not influenced by unknown variables.

In the new biosensor design, assay variances were evaluated by a repeatability study. A standard sample was analyzed 10 times for 50 pg/mL of VEGF standard. The average value, standard deviation, and variation coefficient were 50.2 pg/mL, ±0.74 pg/mL, and 1.47%, respectively. The results of repeatability studies indicated that the biosensor-based technology is very reliable with regard to repeatability. Moreover, the reproducibility of the new biosensor-based VEGF-R1 was also assessed. Twelve biosensors were prepared in a batch and were used for VEGF detection. The calibration curves were also obtained from the impedimetric responses of the 12 biosensors. The results are given in Table 1. The results revealed that the reproducibility of the biosensor based on PAMAM dendrimers was very good.

The stability of the biosensor was also investigated. For this purpose each biosensor was separately stored for between 1 and 20 days under dry conditions at 4 °C. In these studies, the stability was assessed over a 20-day period by performing measurements of 50 pg/mL of VEGF at the end of the fixed storage periods. The results showed that there was no activity decrease at the end of the 15th day. In addition, after 18 days, the biosensor had lost 3.6% of its initial activity, and by the end of the 20th day it had lost about 5.1%.

Finally the proposed VEGF-R1-based biosensor was employed to determine VEGF content in artificial serum samples. The results are displayed in Table 1. The VEGF concentrations of the artificial serum samples analyzed by our proposed biosensor were consistent with that of the spiked amount of it to the serum solutions. The recovery for VEGF was found to be 100.6%.

Conclusion

PAMAM-cysteamine modification was first used as the substrate for the immobilization of VEGF-receptor 1 on a gold electrode with the coupling agent of glutaraldehyde. The fact is that PAMAM-cysteamine SAMs provide a perfect platform for the immobilization of VEGF-receptor-1. Optimized experimental

conditions for the fabrication and operation of the biosensor were studied. The reported biosensor design had a very low detection limit of 5 pg/mL VEGF. The biosensor-based VEGF-R1 showed a good linearity for VEGF determination in a range of 5 to 125 pg/mL. In addition, the experiments revealed that the biosensor showed high sensitivity, repeatability, and reproducibility. The Kramers–Kronig transforms revealed that the whole biosensor system was linear, stable, and formed a causal circuit.

Acknowledgment

The authors gratefully acknowledge the support from TÜBİTAK (The Scientific and Technological Research Council of Turkey, Project number: 109 T 172).

References

[1] J. Sjostrom, C. Blomqvist, P. Heikkila, K.V. Bogulawski, A. Raiseanen-Sokolowski, N.O. Bengtsson, I. Mjaaland, P. Malmstron, B. Ostenstadt, J. Berg, E. Wist, V. Valvere, E. Saksela, Predictive value of p53 mdm-2, p21 and mib-1 for chemotherapy response in advanced breast cancer, Clin. Cancer Res. 6 (8) (2000) 3103–3110.
[2] G. Laguens, S. Coronato, W. Di Girolamo, Biomarkers in breast cancer, Cent. Eur. J. Med. 4 (1) (2006) 330–347.
[3] V. Kulasingam, E.P. Diamandis, Tissue culture-based breast cancer biomarker discovery platform, molecular regulation of vessel maturation, Int. J. Cancer 123 (9) (2008) 2007–2012.
[4] R.K. Jain, Molecular regulation of vessel maturation, Nat. Med. 9 (6) (2003) 685–693.
[5] N. Ferrara, H.P. Gerber, J. LeCouter, The biology of VEGF and its receptors, Nat. Med. 9 (6) (2003) 669–676.
[6] D. Hanahan, J. Folkman, Patterns and emerging mechanisms of the angiogenic switch during tumorigenesis, Cell 86 (3) (1996) 353–364.
[7] C.L. Sawyers, The cancer biomarker problem, Nature 452 (2008) 548–552.
[8] P. Wang, J.R. Whiteaker, A.G. Paulovich, The evolving role of mass spectrometry in cancer biomarker discovery, Cancer Biol. Ther. 8 (12) (2009) 1083–1094.
[9] P. Boffetta, Exploring a cancer biomarker: the example of C-reactive protein, J. Natl. Cancer Inst. 102 (3) (2010) 142–143.
[10] A. Sidoni, G.A. Cavalieri, G. D'Amico, G. Brachelente, E. Bucchiarelli, Biopathological significance of single cell DNA aneuploidy measured by static cytometry in breast cancer, Breast 10 (2001) 325–329.
[11] B. Linderholm, K. Grankvist, N. Wilking, M. Johansson, B. Tavelin, R. Henriksson, Correlation of vascular endothelial growth factor content with recurrences, survival, and first relapse site in primary node-positive breast carcinoma after adjuvant treatment, J. Clin. Oncol. 18 (7) (2000) 1423–1431.
[12] A. Gown, S.E. Rivskin, H.N. Hunt, N.L. Polissar, S.C. Davies, M.K. Atwood, R.J. Tickman, M. Mickel, Prognostic factor of vascular endothelial growth factor (VEGF) expression in node-positive breast cancer, Proc. Am. Soc. Clin. Oncol. 20 (2001) 1703 (abstract).
[13] J.A. Foekens, H.A. Peters, N. Grebenchtchikov, M.P. Look, M.E. Meijer-van Gelder, A. Geurts-Moespot, T.H. van der Kwast, C.G.J. Sweep, J.G.M. Klijn, High tumor levels of vascular endothelial growth factor predict poor response to systemic therapy in advanced breast cancer, Cancer Res. 61 (14) (2001) 5407–5414.
[14] J. Adams, P.J. Carder, S. Downey, M.A. Forbes, K. MacLennan, V. Allgar, S. Kaufman, S. Hallam, R. Bicknell, J.J. Walker, F. Cairnduff, P.J. Selby, T.J. Perren, M. Lansdown, R.E. Banks, Vascular endothelial growth factor (VEGF) in breast cancer: comparison of plasma, serum and tissue VEGF and microvessel density and effects of tamoxifen, Cancer Res. 60 (2000) 2898–2905.
[15] R.S. Rampaul, S.E. Pinder, R.I. Nicholson, W.J. Gullick, J.F. Robertson, I.O. Ellis, Clinical value of epidermal growth factor receptor expression in primary breast cancer, Adv. Anat. Pathol. 12 (2005) 271–273.
[16] H.W. Lo, S.C. Hsu, M.C. Hung, EGFR signaling pathway in breast cancers: from traditional signal transduction to direct nuclear translocalization, Breast Cancer Res. Treat. 28 (2005) 1–8.
[17] H. Rochefort, M. Garcia, M. Glondu, V. Laurent, E. Liaudet, J. Rey, P. Roger, Cathepsin d in breast cancer: mechanisms and clinical applications a 1999 Overview, Clin. Chim. Acta 291 (2000) (1999) 157–170.
[18] V.V. Levenson, Biomarkers for early detection of breast cancer: what, when, and where?, Biochim Biophy. Acta 1770 (2007) 847–856.
[19] R.A. Oldenburg, H. Meijers-Heijboer, C.J. Cornelisse, P. Devilee, Genetic susceptibility for breast cancer: how many more genes to be found?, Crit Rev. Oncol. Hematol. 63 (2007) 125–149.
[20] H.R. Byon, H.C. Choi, Network single-walled carbon nanotube-field effect transistors (SWNT-FETs) with increased Schottky contact area for highly sensitive biosensor applications, J. Am. Chem. Soc. 128 (2006) 2188–2189.
[21] Y. Cui, Q. Wei, H. Park, C.M. Lieber, Nanowire nanosensors for highly sensitive and selective detection of biological and chemical species, Science 293 (17) (2001) 1289–1292.
[22] Z. Gao, A. Agarwal, A.D. Trigg, N. Singh, C. Fang, C.-H. Tung, Y. Fan, K.D. Buddharaju, J. Kong, Silicon nanowire arrays for label-free detection of DNA, Anal. Chem. 79 (2007) 3291–3297.
[23] J. Hahm, C.M. Lieber, Direct ultrasensitive electrical detection of DNA and DNA sequence variations using nanowire nanosensors, Nano Lett. 4 (2004) 51–54.
[24] A. Kim, C.S. Ah, H.Y. Yu, J.-H. Yang, I.-B. Baek, C.-G. Ahn, C.W. Park, M.S. Jun, S. Lee, Ultrasensitive, label-free, and real-time ımmunodetection using silicon field-effect transistors, Appl. Phys. Lett. 91 (2007) 103901–103903.
[25] F. Patolsky, G. Zheng, O. Hayden, M. Lakadamyali, X. Zhuang, C.M. Lieber, Electrical detection of single viruses, Proc. Natl. Acad. Sci. USA 101 (2004) 14017–14022.
[26] E. Stern, J.F. Klemic, D.A. Routenberg, P.N. Wyrembak, D.B. Turner-Evans, A.D. Hamilton, D.A. LaVan, T.M. Fahmy, M.A. Reed, Label-free ımmunodetection with CMOS-compatible semiconducting nanowires, Nature 445 (2007) 519–522.
[27] H.-S. Lee, K.S. Kim, C.-J. Kim, S.K. Hahn, M.H. Jo, Electrical detection of VEGFs for cancer diagnoses using anti-vascular endothelial growth factor aptamer modified Si nanowire FETs, Biosens. Bioelectron. 24 (6) (2009) 1801–1805.
[28] S. Prabhulkar, S. Alwarappan, G. Liu, C.-Z. Li, Amperometric micro-immunosensor for the detection of tumor biomarker, Biosens. Bioelectron. 24 (12) (2009) 3524–3530.
[29] A.W. Bott, Electrochemical techniques for the characterization of redox polymers, Curr. Sep. 19 (2001) 71–75.
[30] E. Katz, I. Willner, Probing biomolecular interactions at conductive and semiconductive surfaces by impedance spectroscopy: routes to impedimetric immunosensors, DNA sensors and enzyme biosensors, Electroanalysis 15 (2003) 913–947.
[31] J.G. Guan, Y.Q. Miao, Q.J. Zhang, Impedimetric biosensors, J. Biosci. Bioeng. 97 (4) (2004) 219–226.
[32] M. Shibuya, S. Yamaguchi, A. Yamane, T. Ikeda, A. Tojo, H. Matsushime, M. Sato, Nucleotide sequence and expression of a novel human receptor-type tyrosine kinase gene (flt) closely related to the fms family, Oncogene 5 (4) (1990) 519–524.
[33] R.L. Kendall, K.A. Thomas, Inhibition of vascular endothelial cell growth factor activity by an endogenously encoded soluble receptor, Proc. Natl. Acad. Sci. USA 90 (22) (1993) 10705–10709.
[34] G. Neufeld, T. Cohen, S. Gengrinovitch, Z. Poltorak, Vascular endothelial growth factor (VEGF) and its receptors, FASEB J. 13 (1) (1999) 9–22.
[35] Y. He, S.K. Smith, K.A. Day, D.E. Clark, D.R. Licence, D.S. Charnock-Jones, Alternative splicing of vascular endothelial growth factor (VEGF)-R1 (FLT-1) pre-mRNA ıs ımportant for the regulation of VEGF activity, Mol. Endocrinol. 13 (4) (1999) 537–545.
[36] B. Olofsson, E. Korpelainen, M.S. Pepper, S.J. Mandriota, K. Aase, V. Kumar, Y. Gunji, M.M. Jeltsch, M. Shibuya, K. Alitalo, U. Eriksson, Vascular endothelial growth factor B (VEGF-B) binds to VEGF receptor-1 and regulates plasminogen activator activity in endothelial cells, Proc. Natl. Acad. Sci. USA 95 (20) (1998) 11709–11714.
[37] G. Conn, D.D. Soderman, M.T. Schaeffer, M. Wile, V.B. Hatcher, K.A. Thomas, Purification of a glycoprotein vascular endothelial cell mitogen from a rat glioma-derived cell line, Proc. Natl. Acad. Sci. USA 87 (4) (1990) 1323–1327.
[38] L. Alfonta, E. Katz, I. Willner, Sensing of acetylcholine by a tricomponentenzyme layered electrode using faradaic impedance spectroscopy, cyclic voltammetry, and microgravimetric quartz crystal microbalance transduction methods, Anal. Chem. 72 (2000) 927–935.
[39] A.J. Bard, L.R. Faulkner, Electrochemical Methods: Fundamentals and Applications, Wiley, New York, 2001.
[40] R.de.L. Kronig, On the theory of dispersion of X-rays, J. Opt. Soc. Am. Rev. Sci. Inst. 12 (1926) 547–557.
[41] H.A. Kramers, Die dispersion und absorption von Rontgenstrahlen, Phys. Z. 30 (1929) 522–523.
[42] M.E. Orazem, B. Tribollet, Electrochemical Impedance Spectroscopy, Wiley, NJ, 2008.
[43] Q.-A. Huang, R. Hui, B. Wang, J. Zhang, A review of AC ımpedance modeling and validation in SOFC diagnosis, Electrochim. Acta 52 (2007) 8144–8164.
[44] W. Ehm, H. Gohr, R. Kaus, B. Roseler, C.A. Schiller, The evaluation of electrochemical ımpedance spectra using a modified logarithmic Hilbert transform, ACH-Models Chem. 137 (2000) 145–157.
[45] B.A. Boukamp, A linear Kronig–Kramers transform test for ımmittance data validation, J. Electrochem. Soc. 142 (1995) 1885–1894.